CHEMISTRY OF MATERIALS
Article
Cite This: Chem. Mater. 2017, 29, 9456-9462
pubs.acs.org/cm

Theoretical Study of Ripening Mechanisms of Pd Clusters on Ceria

Ya-Qiong Su, Jin-Xun Liu, Ivo A. W. Filot, and Emiel J. M. Hensen*

Laboratory of Inorganic Materials Chemistry, Schuit Institute of Catalysis, Eindhoven University of Technology, P.O. Box 513, 5600 MB Eindhoven, The Netherlands

Supporting Information

ABSTRACT: We carried out density functional theory calculations to investigate the ripening of Pd clusters on $CeO_2(111)$. Starting from stable Pd_n clusters (n = 1–21), we compared how these clusters can grow through Ostwald ripening and coalescence. As Pd atoms have mobility higher than that of Pd_n clusters on the $CeO_2(111)$ surface, Ostwald ripening is predicted to be the dominant sintering mechanism. Particle coalescence is possible only for clusters with less than 5 Pd atoms. These ripening mechanisms are facilitated by adsorbed CO through lowering barriers for the cluster diffusion, detachment of a Pd atom from clusters, and transformation of initial planar clusters.

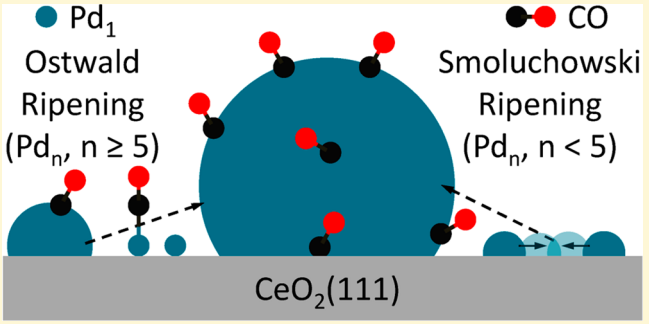

INTRODUCTION

Metal nanoparticles dispersed on high surface area oxide supports are widely applied as catalysts in diverse technology areas such as energy conversion, chemicals manufacture, and environmental protection.[1] Considerable effort has been devoted to understanding the influence of the nanoparticle size on catalytic performance.[2−4] The active phase can vary in size from isolated metal atoms or clusters of a few atoms up to nanoparticles containing thousands of atoms.[5−7] A usual deactivation mechanism of supported nanoparticle catalysts is sintering, as it causes an undesired reduction in metal surface area. Sintering is usually thought to involve either particle migration (Smoluchowski ripening), in which nanoparticles diffuse over the surface and coalesce with other particles, or atomic migration, in which atoms of the nanoparticles are detached and diffuse over the support to attach to another nanoparticle.[8,9] The latter mechanism is well-known as Ostwald ripening, and the main driving force is the minimization of the excess surface free energy. Based on the Gibbs−Thomson relation that describes the concentration of atomic species at support sites near a nanoparticle,[10] various mean-field kinetic models for describing the sintering process have been considered.[9,11−16]

Experimental data on nanoparticle sintering usually favor Ostwald ripening as the main sintering mechanism.[9,15] On the other hand, Jak et al. found by scanning tunneling microscopy study that particle coalescence is the main mechanism for the sintering of very small Pd particles supported on TiO_2.[15] Datye and co-workers mention that particle coalescence can be relevant at high temperature and for nanoparticles in close proximity on an oxide support.[9] It has also been observed that common adsorbates such as CO can affect the sintering process.[17,18] Ouyang et al. showed the importance of metal−carbonyl complexes in atomic transport pathways during Ostwald ripening but also mentioned their role in the redispersion of supported metal nanoparticles.[17]

Ceria is extensively used as a support material mainly because of its high oxygen storage capacity.[19] The primary application of ceria-based catalysts is in automotive three-way convertor technology, which is essential to the cleanup of gasoline engine exhaust gas.[20−22] Pd is now frequently used as a cheaper alternative to Pt for catalyzing CO and hydrocarbon oxidation.[23−25] As thermal sintering of the active phase contributes to the deactivation of these catalysts, it is important to gain a deep understanding of the sintering mechanisms of initially highly dispersed Pd/CeO_2 systems. Ceria as a support is also known for the unusual sinter resistance of noble metals supported on its $CeO_2(111)$ surface.[26] The agglomeration of Pd on ceria has not yet been investigated with atomic-level precision. This can among other ways be achieved by quantum-chemical calculations as, for instance, those shown for the sintering of initially highly dispersed Pt on TiO_2.[27] Although isolated Pd atoms on ceria display promising low-temperature performance,[28] sintering during occasional high-temperature operation will cause sintering and reduced catalytic performance. Accordingly, it is interesting to investigate the ripening mechanism of Pd on ceria.

In the present work, we employed density functional theory (DFT) to determine the stability and mobility of isolated Pd atoms and Pd_n clusters (n = 2–21) on $CeO_2(111)$, which is the most stable surface termination of ceria.[8] On the basis of activation barriers for the migration of such adsorbed atoms and clusters, we discuss possible ripening mechanisms for Pd/

Received: August 22, 2017
Revised: October 13, 2017
Published: October 13, 2017

DOI: 10.1021/acs.chemmater.7b03555
Chem. Mater. 2017, 29, 9456−9462

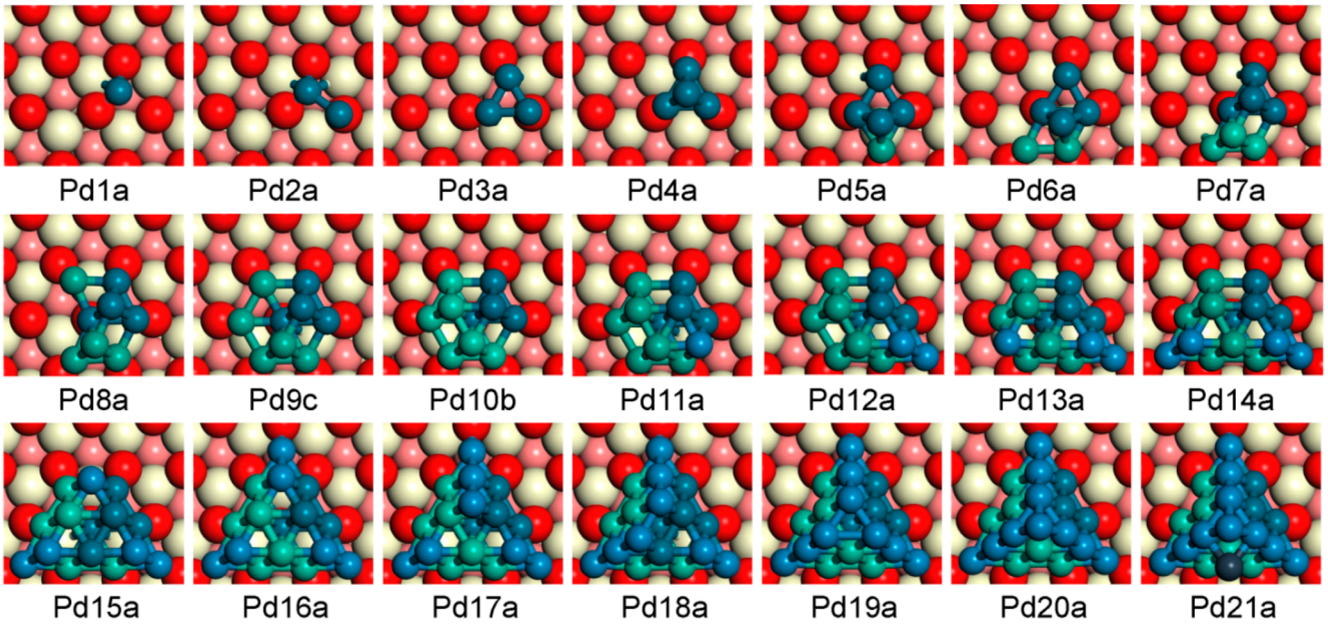

Figure 1. Stable Pd_n clusters (n = 1−21) on the $CeO_2(111)$ surface (color code: red, surface O; light yellow, Ce; coral, subsurface O; dark cyan, 1st−4th Pd; green, 5th−10th Pd; blue, 11th−20th Pd; black, 21st Pd).

CeO_2. We also investigated the role of CO as an adsorbate on the sintering process.

COMPUTATIONAL DETAILS

We carried out spin-polarized calculations within the DFT framework as implemented in the Vienna ab initio simulation package (VASP).[29] The ion-electron interactions are represented by the projector-augmented wave (PAW) method[30] and the electron exchange-correlation by the generalized gradient approximation (GGA) with the Perdew−Burke−Ernzerhof (PBE) exchange-correlation functional.[31] The Kohn−Sham valence states were expanded in a plane-wave basis set with a cutoff energy of 400 eV. The Ce(5s,5p,6s,4f,5d), O(2s,2p), Pd(4d5s), and C(2s,2p) electrons were treated as valence states. The DFT+U approach was used, in which U is a Hubbard-like term describing the on-site Coulombic interactions.[32] This approach improves the description of localized states in ceria, where standard LDA and GGA functionals fail. For Ce, a value of U = 4.5 eV was adopted, which was calculated self-consistently by Fabris et al.[33] using the linear response approach of Cococcioni and de Gironcoli[34] and which is within the 3.0−4.5 eV range that results in the localization in Ce 4f orbitals of the electrons left upon oxygen removal from ceria.[35]

For $Pd_n/CeO_2(111)$ calculations, the model was a periodic ceria slab with a (4 × 4) surface unit cell. For Brillouin zone integration, a 1 × 1 × 1 Monkhorst−Pack mesh was used. The bulk equilibrium lattice constant (5.49 Å) previously calculated at the PBE+U level (U = 4.5 eV) was used.[36] The $CeO_2(111)$ slab model is two Ce−O−Ce layers thick, and the vacuum gap was set to 15 Å. The atoms in the bottom layer were frozen to their bulk positions, and only the top Ce−O−Ce layers were relaxed. The climbing image nudged-elastic band (CI-NEB) algorithm[37,38] was used to identify the transition states for the migration of Pd over the surface and CO oxidation mechanism for selected models.

For reference purposes, we examined gas-phase Pd_n clusters with n = 2−20, 38, 55, 85, 146, and 231. Their initial structures were taken from literature,[7,39−48] and their geometry was further optimized (Figure S1). For these gas-phase Pd_n clusters, the cohesive energy (E_{coh}) was computed via

$$E_{coh} = \frac{nE_{Pd} - E_{Pdn}}{n} \quad (1)$$

Figure S2 shows the relation between the E_{coh} and the number of atoms in the cluster (E_{coh} vs. $n^{-1/3}$).[48] Extrapolation to large n results in an estimate of the bulk cohesive energy at 4.27 eV, in reasonable agreement with the experimental value of 3.9 eV.[49]

For the generation of Pd_n species (n = 1−21) on $CeO_2(111)$, we started from several stable geometries identified for supported Pd_{n-1} clusters (initially starting from Pd_1/CeO_2) and explored stable geometries upon addition of the nth Pd atom. This approach has already been adopted to investigate the polymorphism of gold nanoclusters on a reduced ceria surface.[50] The interface of the largest Pd_{21} cluster with the ceria surface is small enough to be accommodated in a (4 × 4) unit cell. For a Pd_{41} cluster, we considered a larger (6 × 6) supercell.

For Pd_n clusters supported on the $CeO_2(111)$ surface, the cohesive energy can be obtained by taking into account the adhesional energy between the Pd_n cluster and the $CeO_2(111)$ slab.[51] Then, the cohesive energy per Pd atom for the supported Pd_n cluster can be computed from

$$E_{coh} = \frac{nE_{Pd} + E_{ceria} - E_{Pdn-ceria}}{n} \quad (2)$$

The stability of Pd_n clusters on $CeO_2(111)$ was evaluated by computing the energy involved to detach one Pd atom (E_{det}) considering reactions of the type

$$Pd_n - ceria + ceria \rightarrow Pd_{(n-1)} - ceria + Pd - ceria \quad (3)$$

resulting in

$$E_{det} = E_{Pd(n-1)-ceria} + E_{Pd-ceria} - E_{Pdn-ceria} - E_{ceria} \quad (4)$$

In these formulas, E_{Pd}, E_{Pdn}, E_{ceria} and $E_{Pdn-ceria}$ are the electronic energies of an isolated Pd atom, the Pd_n cluster, the empty stoichiometric $CeO_2(111)$ surface, and the $Pd_n/CeO_2(111)$ model, respectively.

RESULTS AND DISCUSSION

Structure of Pd_n Clusters on $CeO_2(111)$ (n = 1−21, 41). We tackled the problem of identifying stable structures by adding Pd atom by atom to stable supported Pd_n clusters starting from optimized $Pd_1/CeO_2(111)$. We determined the most stable configuration for each ceria-supported Pd_n cluster from several candidates. Figure 1 shows the structures of optimized Pd_n clusters on the $CeO_2(111)$ surface. Other configurations and the corresponding energy differences are

DOI: 10.1021/acs.chemmater.7b03555
Chem. Mater. 2017, 29, 9456−9462

collected in Figure S3a. The cohesive energies for the Pd_n clusters with n = 1−21 are given in Figure 2.

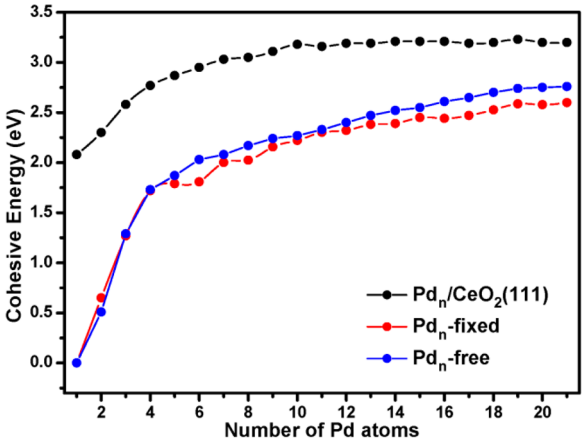

Figure 2. Cohesive energies of ceria-supported Pd (black), the same Pd clusters after removal of the ceria support (red), and corresponding gas-phase clusters (blue).

A Pd atom preferentially adsorbs close to an O-hollow site between two O anions of the $CeO_2(111)$ surface (*Pd1a*). The adsorption energy is 2.08 eV, which is substantially lower than the cohesive energy of bulk Pd. The cohesive energy for the Pd_2 cluster is 2.30 eV. Two stable locations for the Pd_3 cluster were found. Adsorbing Pd_3 at the O-hollow site (*Pd3a*) is more stable than placing it at the Ce-hollow site (*Pd3b*). The three-dimensional tetrahedral Pd_4 cluster (*Pd4a*) is 0.18 eV more stable than its planar counterpart (*Pd4c*), which shows that Pd binds stronger to other Pd atoms than to the interface of the cluster and the ceria support.

A stable Pd_5 cluster is obtained by adding a Pd atom to the Pd_4 cluster in the Ce-hollow site of the ceria surface (*Pd5a*). Another nearly equally stable structure involves migration of the additional Pd atom in the top layer to a location above the Ce-hollow site (*Pd5b*). This migration is very easy with a barrier lower than 0.10 eV. The preferred structure of Pd_6 is derived from Pd_5 by adsorbing a Pd atom in a O-hollow site of the ceria surface (*Pd6a*). The cohesive energy of this cluster is 2.95 eV. The seventh Pd atom can be placed on one of the available threefold Pd sites at the interface formed by the five Pd atoms (*Pd7a*). Placement of the seventh Pd atom on the surface Ce-hollow site (*Pd7c*) is 0.39 eV less favorable. The eighth Pd atom is used to complete the filling of the three threefold sites on the Pd_5 layer (*Pd8a*) or by placing it on the ceria surface (*Pd8b*). These two states have almost the same energy. The ninth Pd atom completes the formation of a Pd_7 hexagon at the ceria surface with two Pd atoms adsorbed in the second layer (*Pd9c*). It should be noted that there is a slightly more stable structure (*Pd9a*, ΔE = −0.14 eV). We show the slightly less stable structure for Pd_9, as the structure of the favorable Pd_{10} cluster (*Pd10b*) is derived from it. Adding the tenth Pd atom to the more stable Pd_9 cluster results in a quite unfavorable structure (*Pd10c*), nearly 1 eV less stable than the most stable Pd_{10} cluster (*Pd10a*). *Pd10b* is 0.08 eV less stable than *Pd10a*. The cohesive energy of the most stable Pd_{10} cluster is 3.18 eV. The 11th Pd atom is located on a 4-fold site of the Pd_{10} cluster (*Pd11a*), a configuration that is 0.24 eV more stable than the one obtained by adsorption adjacent to the cluster on the surface O-hollow site (*Pd11c*). The twelfth Pd atom is preferentially located on the ceria surface in an O-hollow site coordinating to the 11th Pd atom (*Pd12a*) instead of adsorbing on one of the remaining 4-fold site of the Pd_{11} cluster (*Pd12c*). Such structures are less stable by 0.32 eV. Addition of further Pd atoms follows the same sequence until Pd_{16}, i.e., first, a Pd atom is added to a fourfold site followed by placement of another Pd atom on the ceria surface coordinating to this atom. This leads to formation of a symmetric Pd_{16} cluster with a bilayer structure, the first layer consisting of 10 atoms, the second one of 6 atoms (*Pd16a*). The next three Pd atoms can be placed on threefold Pd sites, the twentieth at the resulting threefold site of the Pd_{19} cluster (*Pd20a*). The twenty-first Pd atom is placed on a hollow site of the supported Pd_{20} cluster (*Pd21a*), distant from the surface. We verified that placing the optimized gas-phase Pd_{19} cluster on the ceria surface (*Pd19b*) yielded a structure that was substantially 1.77 eV less stable than the Pd_{19} cluster optimized on the ceria surface. Conversely, the supported Pd_{21} cluster is much less stable than the optimum gas-phase Pd_{21} cluster.

Figure 2 shows that the cohesive energy increases strongly with increasing Pd cluster size up to a 10 Pd atoms. The cohesive energy for clusters between 11 and 20 atoms is nearly constant. The reason is that the number of Pd atoms forming Pd−O bonds with the ceria support is seven for all of these clusters. Although with growing cluster size there are more Pd atoms in the bottom layer, the Pd−O bond distances are much longer (∼2.20 Å) as compared to the other Pd−O distances (∼2.07 Å). We also constructed a Pd_{41} cluster according to the same approach outlined above (see Figure S3a). After placing this cluster on a slightly larger ceria surface unit cell to reduce lateral interactions between the periodic images of these large particles, we found that it also forms seven strong Pd−O bonds. Its cohesive energy is 0.13 eV higher than that of the Pd_{21} cluster, showing that the cohesive energy only slowly approaches the cohesive energy of bulk Pd.

We also examined the cohesive energy of the optimized clusters on the ceria support after removing the ceria support shown in Figure 2. The resulting values are substantially lower than the cohesive energies for the corresponding clusters supported on ceria. The difference, which includes the influence of the adhesion of the Pd cluster on ceria, becomes smaller for larger clusters. Figure 2 also shows the cohesive energies of optimized gas-phase clusters. These are slightly higher than those of the free Pd clusters taken from the ceria support, indicating that the supported cluster adopts a slightly less favorable structure under the influence of the support.

Sintering. We first computed the activation barrier for the migration of a single Pd atom on the $CeO_2(111)$ surface from its most stable site to an adjacent site. The low computed barrier of 0.14 eV implies that the diffusion of atomic Pd in the Ostwald ripening mechanism is very facile. This result is similar to the low barrier reported for the diffusion of a Pd atom on Al_2O_3 surface by Sautet and co-workers.[13] It is interesting to mention that the oxidation of a single Pd atom can stabilize the Pd atom at the ceria surface. We found that the barrier for diffusion of a PdO_2 cluster adsorbed on $CeO_2(111)$ is 0.91 eV, substantially higher than the barrier for diffusion of a Pd atom.[28] Relevant to Ostwald ripening is the energy needed to detach a Pd atom from a cluster and place it on the ceria support.

Figure 3 shows the energy cost to detach a Pd atom from Pd_n clusters adsorbed on the $CeO_2(111)$ surface and place it on the $CeO_2(111)$ surface at infinite distance of the remaining cluster.

DOI: 10.1021/acs.chemmater.7b03555
Chem. Mater. 2017, 29, 9456−9462

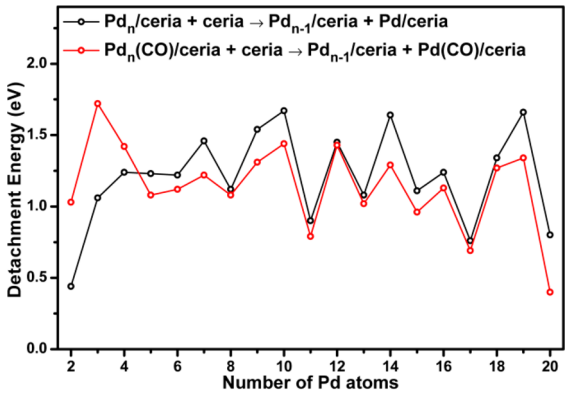

Figure 3. Detachment energies of a Pd atom from ceria-supported Pd$_n$ clusters (n = 2–20) in the absence and presence of CO.

The lowest detachment energy is for the Pd_2 cluster (~0.4 eV), while clusters containing 11, 17, and 20 atoms also have detachment energies below 1 eV. The highest detachment energies (~1.7 eV) are for Pd_{10}, Pd_{14}, and Pd_{19} clusters. These data show that some clusters are more stable than others. Adsorption of CO on the supported clusters can facilitate this process. CO adsorption lowers the detachment energy for clusters with more than 4 Pd atoms. For this, we assumed that CO remains adsorbed on the detached Pd atom. The reason for the lower detachment energy in the presence of CO is the stronger binding of CO to a single Pd atom (E_{ads} = −2.40 eV) in comparison to Pd clusters with more than 4 Pd atoms, which have a CO adsorption energy between −2.00 and −2.40 eV. Recently, Li et al. used molecular dynamics simulations to show that CO can promote single gold atom detachment from Au$_n$ clusters supported on a ceria surface.[52] Accordingly, we expect that such process can also occur, resulting in formation of isolated Pd-CO species on ceria.

We also considered the migration of whole clusters, which is relevant for particle coalescence. Figure 4 shows two different pathways for the diffusion of the most stable tetrahedral Pd_4 cluster on the $CeO_2(111)$ surface. The diffusion barrier, involving a translational migration of the cluster to a similar adjacent site at the surface is 1.83 eV. We also explored an alternative mechanism in which the cluster rotates in two steps over the surface, as shown in Figure 4a. This migration proceeds with an appreciably lower overall barrier of 1.35 eV compared to that of translation migration. For the rotational mechanism, we also explored how CO adsorption to the Pd_4 cluster influences the migration process. In the presence of one coadsorbed CO on a hollow site of the supported Pd_4 cluster, the barrier decreased to 1.03 eV (Figure S5). We expect that adsorption of more CO molecules will further facilitate this migration process.

We also determined activation barriers for these two mechanisms for supported Pd_2, Pd_3, Pd_7, and Pd_{10} clusters (see Figures S6–S9 in the Supporting Information). Figure 5 shows the strong correlation between the barrier and the number of Pd atoms in the cluster. We also added the Pd atom to the correlation for the two-step mechanism because its diffusion also involves two steps with barriers of 0.06 and 0.14 eV. The latter value is the overall barrier reported in Figure 5. These correlations indicate that the two-step mechanism is preferred over the direct one.

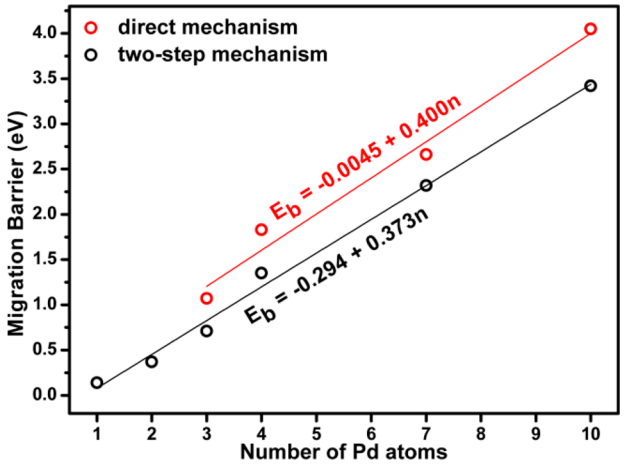

Figure 5. Migration barrier for Pd$_n$ cluster migration via the direct mechanism (red) and the two-step mechanism involving cluster rotation (black) against the number of Pd atoms in the clusters.

Overall, the presented data show that Ostwald ripening will be the more likely sintering mechanism for Pd clusters dispersed on ceria. This agrees well with experimental findings and results of mean-field kinetic modeling describing nanoparticle sintering on oxide supports.[9,15] For the smallest Pd clusters with 2 and 3 atoms, the migration barriers (0.37 and 0.71 eV, respectively) are lower than the detachment energies of these clusters (0.44 and 1.06 eV, respectively). The detachment energy for the Pd_4 cluster is lower than the barrier for migration over the ceria surface. On the other hand, CO can

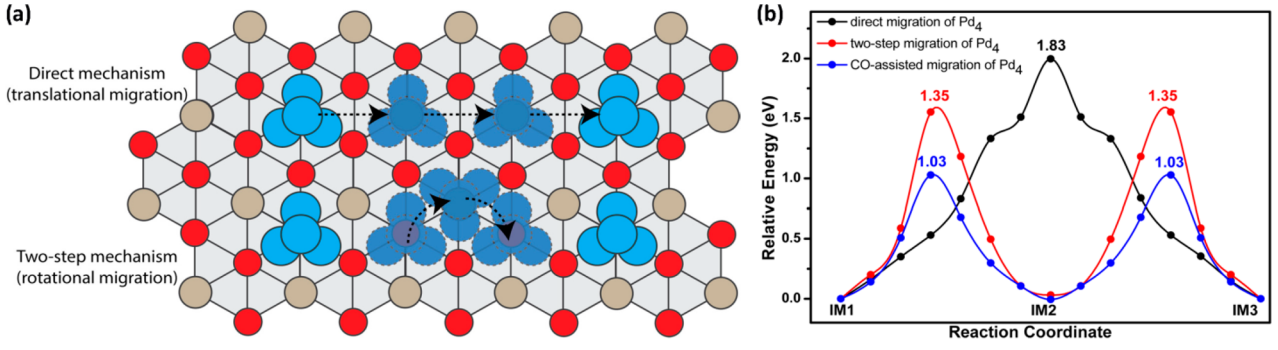

Figure 4. (a) Migration mechanism of a Pd_4 cluster via a direct translation mechanism and a two-step mechanism involving rotational migration. (b) Potential energy diagrams for the migration of a stable tetrahedral Pd_4 cluster on the $CeO_2(111)$ surface via direct translational migration (black), two-step migration (red), and CO-assisted two-step migration (blue).

DOI: 10.1021/acs.chemmater.7b03555
Chem. Mater. 2017, 29, 9456–9462

facilitate the detachment of Pd, implying that both mechanisms play a role in the sintering of Pd_4 clusters. According to Figure 5, the barrier for Pd_5 migration is 1.57 eV, which is much higher than the detachment energy of a Pd atom (1.23 eV). These results demonstrate that clusters with more than 4 Pd atoms will display only limited mobility on the $CeO_2(111)$ surface. Frenken and co-workers showed that coalescence is preferred for very small Pd clusters on TiO_2.[15] We also showed the importance of adsorbate-induced migration. Adsorption of CO reduces these migration barriers. In addition to CO, Pd can also be covered by O atoms during CO oxidation. On the other hand, as discussed above, oxidation of Pd causes a much lower mobility of isolated Pd atoms.[28]

It is important to point out that Ostwald ripening will initially lead to planar clusters. Planar Pd_2 and Pd_3 clusters are the most stable ones. Adding a fourth Pd atom results in a planar structure, whereas the tetrahedral Pd_4 cluster is more stable. Figure S10 shows the reaction energy diagram for the migration of one of the four Pd atoms in a planar Pd_4 cluster to form a tetrahedral Pd_4 cluster. The activation energy barriers for this transformation in the absence and presence of CO are 0.89 and 0.72 eV, respectively. These values are lower than typical detachment energies for most clusters and, accordingly, we do not expect that such transformation will be the limiting factor in the sintering of highly isolated Pd into three-dimensional nanoparticles.

The current insights about Pd migration and sintering pertain to the most stable surface termination of CeO_2. We speculate that ceria surface defects such as vacancies and steps may stabilize Pd. For instance, Petersen et al. showed that heating Pd supported on La-stabilized alumina results in redispersion of PdO, most likely due to trapping of Pd atoms in surface vacancies.[53] On the other hand, it is predicted that detachment of Pd species from PdO faces high barriers.[54] In this respect, it is worthwhile to emphasize that dispersion of the supported Pd_n clusters in our work to form PdO_2, an intermediate identified in catalytic CO oxidation,[28] is exergonic (Figure S11). We surmise that high temperature oxidation can overcome high activation barriers for the detachment of Pd atoms from large Pd or Pd-oxide clusters. Finally, Datye and co-workers elegantly showed that Pt-oxide can disperse atomically at ceria step-edge sites, essentially implying high-temperature oxidation Ostwald ripening.[55] Inspired by this, we explored the possible trapping of Pd on a stepped $CeO_2(111)$ site. A Pd atom binds very strongly to this ceria surface step (−3.56 eV), and its diffusion barrier along the step is 1.67 eV, much higher than the value of 0.14 eV on the terrace. The diffusion of this Pd atom to the terrace is also difficult with a barrier of 1.58 eV, as shown in Figure 6. It implies that the single Pd atom prefers to bind to ceria defects. Moreover, when a Pd_2 cluster is adsorbed along this step, it spontaneously dissociates into two isolated Pd atoms along the ceria edge (Figure S12).

CONCLUSIONS

In summary, density functional theory was used to clarify the structure and formation through Ostwald ripening and particle coalescence of Pd_n clusters on the most stable (111) termination of ceria. Ostwald ripening is predicted to be the preferred mechanism for growth of the clusters. Small clusters of a few Pd atoms can also migrate and contribute to sintering through particle coalescence. The migration of Pd_n clusters on CeO_2 strongly depends on the number of Pd atoms in clusters. Adsorbed CO facilitates these sintering processes through lowering barriers for the cluster diffusion, detachment of a Pd atom from clusters, and transformation of initial planar clusters. The present work shows how Pd atoms or clusters on CeO_2 are prone to thermal sintering into larger clusters via Ostwald ripening and coalescence involving small clusters.

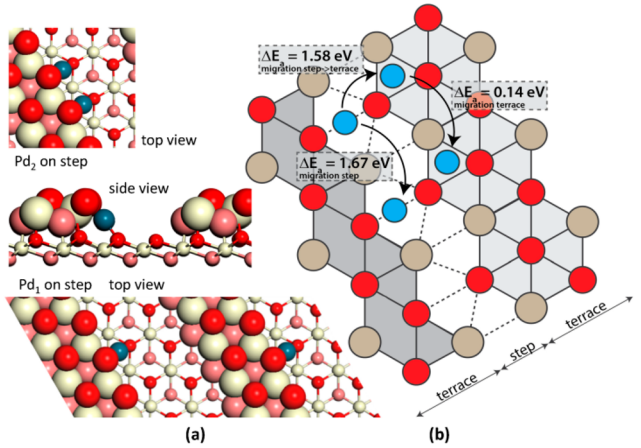

Figure 6. (a) Pd_1 and Pd_2 on steps of $CeO_2(111)$. (b) Diffusion pathways of single Pd atom on step and terrace of $CeO_2(111)$. (Color code: red, surface O of terrace; coral, subsurface O of terrace; light yellow, Ce; dark cyan, Pd).

ASSOCIATED CONTENT

Supporting Information

The Supporting Information is available free of charge on the ACS Publications website at DOI: 10.1021/acs.chemmater.7b03555.

Model construction and parameter settings, optimized Pd_n clusters in gas phase, various candidates of Pd_n clusters on $CeO_2(111)$, and potential energy profiles of Pd_n clusters (n = 1−4, 7, and 10) migration and related intermediates (PDF)

AUTHOR INFORMATION

Corresponding Author

*E-mail: e.j.m.hensen@tue.nl.

ORCID

Jin-Xun Liu: 0000-0002-7499-4197

Emiel J. M. Hensen: 0000-0002-9754-2417

Notes

The authors declare no competing financial interest.

ACKNOWLEDGMENTS

The authors acknowledge financial support for the research from The Netherlands Organization for Scientific Research (NWO) through a Vici grant and Nuffic funding. This project also received funding from the European Union's Horizon 2020 research and innovation programme PARTIAL-PGMs under Grant 686086. Access to supercomputing facilities was provided by NWO.

REFERENCES

(1) Bell, A. T. The Impact of Nanoscience on Heterogeneous Catalysis. *Science* **2003**, *299*, 1688−1691.

(2) Matthey, D.; Wang, J.; Wendt, S.; Matthiesen, J.; Schaub, R.; Lægsgaard, E.; Hammer, B.; Besenbacher, F. Enhanced Bonding of

DOI: 10.1021/acs.chemmater.7b03555
Chem. Mater. 2017, 29, 9456−9462

Gold Nanoparticles on Oxidized TiO_2(110). *Science* **2007**, *315*, 1692−1696.
(3) Vajda, S.; Pellin, M. J.; Greeley, J. P.; Marshall, C. L.; Curtiss, L. A.; Ballentine, G. A.; Elam, J. W.; Catillon-Mucherie, S.; Redfern, P. C.; Mehmood, F.; Zapol, P. Subnanometre Platinum Clusters as Highly Active and Selective Catalysts for the Oxidative Dehydrogenation of Propane. *Nat. Mater.* **2009**, *8*, 213−216.
(4) Kaden, W. E.; Kunkel, W. A.; Kane, M. D.; Roberts, F. S.; Anderson, S. L. Size-Dependent Oxygen Activation Efficiency over Pd_n/TiO_2(110) for the CO Oxidation Reaction. *J. Am. Chem. Soc.* **2010**, *132*, 13097−13099.
(5) Lee, S.; Lee, B.; Mehmood, F.; Seifert, S.; Libera, J. A.; Elam, J. W.; Greeley, J.; Zapol, P.; Curtiss, L. A.; Pellin, M. J. Oxidative Decomposition of Methanol on Subnanometer Palladium Clusters: the Effect of Catalyst Size and Support Composition. *J. Phys. Chem. C* **2010**, *114*, 10342−10348.
(6) Lopez-Sanchez, J. A.; Dimitratos, N.; Hammond, C.; Brett, G. L.; Kesavan, L.; White, S.; Miedziak, P.; Tiruvalam, R.; Jenkins, R. L.; Carley, A. F. Facile Removal of Stabilizer-Ligands from Supported Gold Nanoparticles. *Nat. Chem.* **2011**, *3*, 551−556.
(7) Yudanov, I. V.; Genest, A.; Schauermann, S.; Freund, H. J.; Rösch, N. Size Dependence of the Adsorption Energy of CO on Metal Nanoparticles: a DFT Search for the Minimum Value. *Nano Lett.* **2012**, *12*, 2134−2139.
(8) Wanke, S. E.; Flynn, P. C. The Sintering of Supported Metal Catalysts. *Catal. Rev.: Sci. Eng.* **1975**, *12*, 93−135.
(9) Hansen, T. W.; DeLaRiva, A. T.; Challa, S. R.; Datye, A. K. Sintering of Catalytic Nanoparticles: Particle Migration or Ostwald Ripening? *Acc. Chem. Res.* **2013**, *46*, 1720−1730.
(10) Chakraverty, B. Grain Size Distribution in Thin Films—1. Conservative Systems. *J. Phys. Chem. Solids* **1967**, *28*, 2401−2412.
(11) Voorhees, P. W. The Theory of Ostwald Ripening. *J. Stat. Phys.* **1985**, *38*, 231−252.
(12) Campbell, C. T.; Parker, S. C.; Starr, D. E. The Effect of Size-Dependent Nanoparticle Energetics on Catalyst Sintering. *Science* **2002**, *298*, 811−814.
(13) Datye, A. K.; Xu, Q.; Kharas, K. C.; McCarty, J. M. Particle Size Distributions in Heterogeneous Catalysts: What Do They Tell Us about the Sintering Mechanism? *Catal. Today* **2006**, *111*, 59−67.
(14) Simonsen, S. B.; Chorkendorff, I.; Dahl, S.; Skoglundh, M.; Sehested, J.; Helveg, S. Ostwald Ripening in a Pt/SiO_2 Model Catalyst Studied by in Situ TEM. *J. Catal.* **2011**, *281*, 147−155.
(15) DeLaRiva, A. T.; Hansen, T. W.; Challa, S. R.; Datye, A. K. In Situ Transmission Electron Microscopy of Catalyst Sintering. *J. Catal.* **2013**, *308*, 291−305.
(16) Asoro, M.; Ferreira, P.; Kovar, D. In Situ Transmission Electron Microscopy and Scanning Transmission Electron Microscopy Studies of Sintering of Ag and Pt Nanoparticles. *Acta Mater.* **2014**, *81*, 173−183.
(17) Ouyang, R.; Liu, J.-X.; Li, W. X. Atomistic Theory of Ostwald Ripening and Disintegration of Supported Metal Particles under Reaction Conditions. *J. Am. Chem. Soc.* **2013**, *135*, 1760−1771.
(18) Suzuki, A.; Inada, Y.; Yamaguchi, A.; Chihara, T.; Yuasa, M.; Nomura, M.; Iwasawa, Y. Time Scale and Elementary Steps of CO-Induced Disintegration of Surface Rhodium Clusters. *Angew. Chem., Int. Ed.* **2003**, *42*, 4795−4799.
(19) Sun, C.; Li, H.; Chen, L. Nanostructured Ceria-Based Materials: Synthesis, Properties, and Applications. *Energy Environ. Sci.* **2012**, *5*, 8475−8505.
(20) Bera, P.; Patil, K.; Jayaram, V.; Subbanna, G.; Hegde, M. Ionic Dispersion of Pt and Pd on CeO_2 by Combustion Method: Effect of Metal−Ceria Interaction on Catalytic Activities for NO Reduction and CO and Hydrocarbon Oxidation. *J. Catal.* **2000**, *196*, 293−301.
(21) Guzman, J.; Carrettin, S.; Corma, A. Spectroscopic Evidence for the Supply of Reactive Oxygen during CO Oxidation Catalyzed by Gold Supported on Nanocrystalline CeO_2. *J. Am. Chem. Soc.* **2005**, *127*, 3286−3287.
(22) Liu, G.; Gao, P. X. A Review of NO_x Storage/Reduction Catalysts: Mechanism, Materials and Degradation Studies. *Catal. Sci. Technol.* **2011**, *1*, 552−568.
(23) Shen, M.; Yang, M.; Wang, J.; Wen, J.; Zhao, M.; Wang, W. Pd/Support Interface Promoted $Pd-Ce_{0.7}Zr_{0.3}O_2-Al_2O_3$ Automobile Three-Way Catalysts: Studying the Dynamic Oxygen Storage Capacity and CO, C_3H_8, and NO Conversion. *J. Phys. Chem. C* **2009**, *113*, 3212−3221.
(24) Zhu, H.; Qin, Z.; Shan, W.; Shen, W.; Wang, J. Low-Temperature Oxidation of CO over Pd/CeO_2-TiO_2 Catalysts with Different Pretreatments. *J. Catal.* **2005**, *233*, 41−50.
(25) Jamalzadeh, Z.; Haghighi, M.; Asgari, N. Synthesis, Physicochemical Characterizations and Catalytic Performance of Pd/Carbon-Zeolite and Pd/Carbon-CeO_2 Nanocatalysts Used for Total Oxidation of Xylene at Low Temperatures. *Front. Environ. Sci. Eng.* **2013**, *7*, 365−381.
(26) Farmer, J. A.; Campbell, C. T. Ceria Maintains Smaller Metal Catalyst Particles by Strong Metal-Support Bonding. *Science* **2010**, *329*, 933−936.
(27) Zhou, Y.; Muhich, C. L.; Neltner, B. T.; Weimer, A. W.; Musgrave, C. B. Growth of Pt Particles on the Anatase TiO_2(101) Surface. *J. Phys. Chem. C* **2012**, *116*, 12114−12123.
(28) Spezzati, G.; Su, Y. Q.; Hofmann, J. P.; Benavidez, A. D.; Delariva, A. T.; McCabe, J.; Datye, A. K.; Hensen, E. J. M. Atomically Dispersed Pd-O Species on CeO_2(111) as Highly Active Sites for Low-Temperature CO Oxidation. *ACS Catal.* **2017**, *7*, 6887−6891.
(29) Kresse, G.; Hafner, J. Ab Initio Molecular-Dynamics Simulation of the Liquid-Metal−Amorphous-Semiconductor Transition in Germanium. *Phys. Rev. B: Condens. Matter Mater. Phys.* **1994**, *49*, 14251.
(30) Blöchl, P. E. Projector Augmented-Wave Method. *Phys. Rev. B: Condens. Matter Mater. Phys.* **1994**, *50*, 17953.
(31) Perdew, J. P.; Burke, K.; Ernzerhof, M. Generalized Gradient Approximation Made Simple. *Phys. Rev. Lett.* **1996**, *77*, 3865.
(32) Dudarev, S.; Botton, G.; Savrasov, S.; Humphreys, C.; Sutton, A. Electron-Energy-Loss Spectra and the Structural Stability of Nickel Oxide: An LSDA+U Study. *Phys. Rev. B: Condens. Matter Mater. Phys.* **1998**, *57*, 1505.
(33) Fabris, S.; de Gironcoli, S.; Baroni, S.; Vicario, G.; Balducci, G. Reply to "Comment on 'Taming Multiple Valency with Density Functionals: A Case Study of Defective Ceria'. *Phys. Rev. B: Condens. Matter Mater. Phys.* **2005**, *72*, 237102.
(34) Cococcioni, M.; De Gironcoli, S. Linear Response Approach to the Calculation of the Effective Interaction Parameters in the LDA+U Method. *Phys. Rev. B: Condens. Matter Mater. Phys.* **2005**, *71*, 035105.
(35) Castleton, C.; Kullgren, J.; Hermansson, K. Tuning LDA+ U for Electron Localization and Structure at Oxygen Vacancies in Ceria. *J. Chem. Phys.* **2007**, *127*, 244704−244704.
(36) Da Silva, J. L.; Ganduglia-Pirovano, M. V.; Sauer, J.; Bayer, V.; Kresse, G. Hybrid Functionals Applied to Rare-Earth Oxides: The Example of Ceria. *Phys. Rev. B: Condens. Matter Mater. Phys.* **2007**, *75*, 045121.
(37) Henkelman, G.; Jónsson, H. Improved Tangent Estimate in the Nudged Elastic Band Method for Finding Minimum Energy Paths and Saddle Points. *J. Chem. Phys.* **2000**, *113*, 9978−9985.
(38) Sheppard, D.; Terrell, R.; Henkelman, G. Optimization Methods for Finding Minimum Energy Paths. *J. Chem. Phys.* **2008**, *128*, 134106.
(39) Ma, L.; Wang, J.; Wang, G. Dipole Polarizabilities of Pd_N (N= 2−25) Clusters. *Eur. Phys. J. D* **2013**, *67*, 1−9.
(40) Chattaraj, D.; Parida, S. C.; Dash, S.; Majumder, C. Influence of U Doping on the Growth Behavior, Electronic Structure and Magnetic Properties of Pd_n (n = 1−12) Clusters: a First Principles Study. *Eur. Phys. J. D* **2014**, *68*, 1−7.
(41) Viñes, F.; Gomes, J. R.; Illas, F. Understanding the Reactivity of Metallic Nanoparticles: Beyond the Extended Surface Model for Catalysis. *Chem. Soc. Rev.* **2014**, *43*, 4922−4939.
(42) Koitz, R.; Soini, T. M.; Genest, A.; Trickey, S.; Rösch, N. Structure-Dependence of the Magnetic Moment in Small Palladium

DOI: 10.1021/acs.chemmater.7b03555
Chem. Mater. 2017, 29, 9456−9462

Clusters: Surprising Results From the M06-L Meta-GGA Functional. *Int. J. Quantum Chem.* **2012**, *112*, 113−120.
(43) Köster, A. M.; Calaminici, P.; Orgaz, E.; Roy, D. R.; Reveles, J. U.; Khanna, S. N. On the Ground State of Pd_{13}. *J. Am. Chem. Soc.* **2011**, *133*, 12192−12196.
(44) Zhang, H.; Tian, D.; Zhao, J. Structural Evolution of Medium-Sized Pd_n(n= 15−25) Clusters from Density Functional Theory. *J. Chem. Phys.* **2008**, *129*, 114302.
(45) Yudanov, I. V.; Genest, A.; Rösch, N. DFT Studies of Palladium Model Catalysts: Structure and Size Effects. *J. Cluster Sci.* **2011**, *22*, 433−448.
(46) Yudanov, I. V.; Sahnoun, R.; Neyman, K. M.; Rösch, N.; Hoffmann, J.; Schauermann, S.; Johanek, V.; Unterhalt, H.; Rupprechter, G.; Libuda, J.; Freund, H.-J. CO Adsorption on Pd Nanoparticles: Density Functional and Vibrational Spectroscopy Studies. *J. Phys. Chem. B* **2003**, *107*, 255−264.
(47) Wu, X.; Dong, Y. Theoretical Studies of Structures and Energies of Pd, Au−Pd, and Au−Pd−Pt Clusters. *New J. Chem.* **2014**, *38*, 4893−4900.
(48) Nava, P.; Sierka, M.; Ahlrichs, R. Density Functional Study of Palladium Clusters. *Phys. Chem. Chem. Phys.* **2003**, *5*, 3372−3381.
(49) Wagman, D. D.; Evans, W. H.; Parker, V. B.; Schumm, R. H.; Halow, I. *The NBS Tables of Chemical Thermodynamic Properties. Selected Values for Inorganic and C_1 and C_2 Organic Substances in SI Units*, DTIC Document; American Chemical Society and the American Institute of Physics for the National Bureau of Standards: Washington, D.C., 1982.
(50) Zhang, C.; Michaelides, A.; King, D. A.; Jenkins, S. J. Positive Charge States and Possible Polymorphism of Gold Nanoclusters on Reduced Ceria. *J. Am. Chem. Soc.* **2010**, *132*, 2175−2182.
(51) Li, X. Modeling the Size-and Shape-Dependent Cohesive Energy of Nanomaterials and Its Applications in Heterogeneous Systems. *Nanotechnology* **2014**, *25*, 185702.
(52) Liu, J. C.; Wang, Y. G.; Li, J. Toward Rational Design of Oxide-Supported Single-Atom Catalysts: Atomic Dispersion of Gold on Ceria. *J. Am. Chem. Soc.* **2017**, *139*, 6190−6199.
(53) Peterson, E. J.; DeLaRiva, A. T.; Lin, S.; Johnson, R. S.; Guo, H.; Miller, J. T.; Kwak, J. H.; Peden, C. H.; Kiefer, B.; Allard, L. F. Low-Temperature Carbon Monoxide Oxidation Catalysed by Regenerable Atomically Dispersed Palladium on Alumina. *Nat. Commun.* **2014**, *5*, 4885.
(54) Johns, T. R.; Goeke, R. S.; Ashbacher, V.; Thüne, P. C.; Niemantsverdriet, J.; Kiefer, B.; Kim, C. H.; Balogh, M. P.; Datye, A. K. Relating Adatom Emission to Improved Durability of Pt−Pd Diesel Oxidation Catalysts. *J. Catal.* **2015**, *328*, 151−164.
(55) Jones, J.; Xiong, H.; DeLaRiva, A. T.; Peterson, E. J.; Pham, H.; Challa, S. R.; Qi, G.; Oh, S.; Wiebenga, M. H.; Hernández, X. I. P. Thermally Stable Single-Atom Platinum-on-Ceria Catalysts via Atom Trapping. *Science* **2016**, *353*, 150−154.

DOI: 10.1021/acs.chemmater.7b03555
Chem. Mater. 2017, 29, 9456−9462